The Clay Minerals Society Workshop Lectures Series, Vol. 21 (2016), Chapter 9, 105–128

MICROSCOPIC CHEMICAL IMAGING: A KEY TO UNDERSTAND ION MOBILITY IN TIGHT FORMATIONS

D. Grolimund[1]*, H.A.O. Wang[1,2], L.R. van Loon[3], F. Marone[1], N. Diaz[3], A. Kaestner[4], and A. Jakob[3]

[1]*Swiss Light Source (SLS), Paul Scherrer Institute, CH-5232 Villigen-PSI, Switzerland*
[2]*Laboratory for Inorganic Chemistry, ETHZ Zurich, CH-8093 Zurich, Switzerland*
[3]*Laboratory for Waste Management, Paul Scherrer Institute, CH-5232 Villigen-PSI, Switzerland*
[4]*Spallation Neutron Source (SINQ), Paul Scherrer Institute, CH-5232 Villigen PSI, Switzerland*
**e-mail: daniel.grolimund@psi.ch*

Tight clay formations are frequently employed as natural or engineered barrier systems in the context of safe disposal of toxic waste. To evaluate long-term barrier efficiency, understanding the spreading and transport of contaminants in these porous media is of critical importance. Tight clay formations exhibit pronounced physical and chemical heterogeneities at various length scales. These heterogeneities potentially dictate the reactive transport characteristics. Modern micro-analytical techniques such as synchrotron-based micro X-ray fluorescence, X-ray spectromicroscopy or X-ray tomographic microscopy, and neutron imaging techniques, as well as laboratory-based microprobe techniques, can be employed to gain new insights into diffusion processes of reactive chemicals occurring in such multi-domain, micro-structured porous media. In addition to structural information, detailed chemical information can be obtained. Most importantly, these modern methods are capable of providing information from within the porous medium directly illustrating the heterogeneous distribution of chemical properties and their inter-relations. Consequently, combined with the capability to image the reactive transport pattern in up to full three dimensions, heterogeneity-reactivity relationships can be derived. Based on the illustrative example of cesium (Cs) migration in Opalinus Clay rock, multi-dimensional and multi-modal imaging of reactive transport phenomena have demonstrated unequivocally that physical and chemical heterogeneities are indeed transport relevant.

1. Introduction

The safe disposal of toxic waste as well as control of the negative impact of hazardous chemicals are among the most challenging tasks in terms of sustaining the development of modern civilizations. In this context, understanding the spread and transport of contaminants in natural porous media (*e.g.* subsurface environments) is of central importance.

Transport phenomena in natural porous media have been studied extensively, mainly in laboratory studies (*e.g.* Cernik *et al.,* 1994; Kohler *et al.,* 1996; Meeussen *et al.,* 1999;

DOI: 10.1346/CMS-WLS-21.9

Grolimund and Borkovec, 2005; Van Loon *et al.,* 2007; Appelo *et al.,* 2010; Dai *et al.,* 2012; Prigiobbe and Bryant, 2014; Van Loon and Mibus, 2015) and, to a lesser extent, in larger-scale field studies (Geckeis *et al.,* 2004; Wersin *et al.,* 2008; Cvetkovic *et al.,* 2010; Gimmi *et al.,* 2014).

In such experiments, the solute mass flow through, into, or out of a piece of subsurface material is measured as a function of time. Observed mass-flow patterns at the boundaries are generally interpreted by applying the classical Fickian laws assuming an homogeneous and isotropic porous medium. Such an approach yields a set of 'spatially averaged transport parameters' such as diffusion and dispersion coefficients, accessible porosities, *etc*. Such 'lumped' transport parameters are subsequently used in transport predictions or safety assessments, *e.g.* for radioactive-waste repositories. Natural porous media are far from being homogeneous and isotropic, however, but are, instead, a mixture of different mineral conglomerates forming a complex three-dimensional entity. Macroscopic physical properties as well as the chemical reactivity of bulk materials are generally determined by the nature of their micro-domain configuration. This is especially the case when dealing with highly reactive contaminants.

For most chemically active porous materials or composite systems (such as natural or engineered clay systems), their physical structure and chemical reactivity are reflected directly in the spatial distribution of chemical properties. Key properties include chemical composition (distribution of elements and compounds), chemical speciation (atomic coordination of a specific chemical element), and chemical states (*e.g.* redox state). Chemical information provides key information about reactivity as well as about the structural properties of heterogeneous materials. Developing concepts that take into account both the physical and chemical heterogeneity on the micrometer scale is both essential and challenging. Unfortunately, the vast majority of reactive transport studies provide information at the upper and/or lower boundaries of the investigated porous media only. Spatially resolved information, in particular chemical, from within the porous medium is generally not available. The information content is limited to a single or a few points on the object boundary.

To further advance our understanding of the relevant reactive transport processes, however, the replacement of the spatially averaged, homogeneous medium within the scientific conceptualizations used by a realistic, physically and chemically structured representation is critical. Consequently, current demands on imaging extend beyond traditional structural (physical) imaging. The ability to visualize the distribution of chemical properties at the (sub-)micrometer scale as well as chemical reactions and dynamics within materials is of fundamental interest and importance. As a result the need for 'chemical microscopes' is growing rapidly.

2. Microscopic chemical imaging

Over recent years, micro-analytical facilities based on synchrotron X-ray radiation as well as neutron beams have become indispensable in the context of non-destructive micro-analytical imaging. Both types of beams are now used for multi-dimensional

structural micro-analysis (physical imaging) as well as chemical and crystallographic micro-imaging. Because of their generally non-destructive interaction with matter, neutrons and X-rays provide complementary analytical contrast mechanisms.

X-ray microprobe facilities possess several intrinsic advantages in terms of chemical imaging. Most importantly, the element-specific absorption resonances accessible within the wide X-ray energy range provide an element-specific chemical sensitivity. Moreover, the fine structure of an absorption edge reveals information about the chemical speciation (molecular environment) of the absorber. Different oxidation states are identified readily, in many cases, based on their characteristic spectroscopy signatures of the absorption edges. Furthermore, any specific chemical environment around the absorber will potentially lead to specific bound-bound transitions at the low-energy side of the edge, while the coordination geometry will result in characteristic scattering phenomena above the Fermi level reflected in spectroscopic signatures at the high-energy side of the edge. These speciation-dependent features represent chemical contrast which can be used to record up to three-dimensional chemical images documenting the spatial variation of oxidation states, specific mineral phases, or different molecular species (*e.g.* Bertsch and Hunter, 2001; Trainor *et al.,* 2006; Baruchel *et al.,* 2008; Margaritondo *et al.,* 2008; Bleuet *et al.,* 2010; Marcus, 2010).

Complementary to X-rays, a neutron beam exhibits a unique penetration power, a particular sensitivity for certain low-Z elements, as well as isotope sensitivity. Neutron radiography and tomography are the most suitable non-destructive tools for dense objects when a certain size of the object is reached (Anderson *et al.,* 2009; Banhart *et al.,* 2010). In contrast to the more common X-ray approaches, even bulk materials with heavy elements can be penetrated. Moreover, due to the large cross section of low-Z elements, light-element materials can be distinguished from each other and small amounts of aqueous liquids or organic materials can be detected with a high contrast even within a dense body. Neutron imaging is a highly specialized method which allows the observation of hidden structures and features in bulk objects (Lehmann *et al.,* 2006; Liang *et al.,* 2009; Lehmann *et al.,* 2014; Kaestner *et al.,* 2015; Schrofl *et al.,* 2015).

Recent progress has also been noted in terms of laboratory-based microprobe techniques used to study the chemical micro-heterogeneity of natural or engineered materials. As an example, laser ablation inductively coupled plasma mass spectrometry (LA-ICP-MS) has recently evolved into a powerful imaging tool for the qualitative and quantitative microscale imaging of solid materials (Kindness *et al.,* 2003; Wang *et al.,* 2013; Giesen *et al.,* 2014).

Additional laboratory-based microprobe techniques (although not employed in the present study) are capable of acquiring images containing chemical information. Examples include, among others, laser-induced breakdown spectroscopy (LIBS) imaging (Pinon *et al.,* 2013; Sancey *et al.,* 2014), nano-secondary ion mass spectrometry (nano-SIMS) (Herrmann *et al.,* 2007), particle-induced X-ray emission spectrometry (PIXE) (Johansson *et al.,* 1995), scanning electron spectroscopy (SEM) coupled to energy-dispersive X-ray spectroscopy (EDS or EDX) and electron microprobe analysis (EMPA) (Goldstein *et al.,* 2003; Reed, 2010), infrared (IR) microscopy (Katon, 1996; Hirschmugl and Gough, 2012), Raman spectroscopy (Truchet *et al.,* 1996; Dieing

et al., 2011), or X-ray photoelectron spectroscopy (XPS), also referred to as electron spectroscopy for chemical analysis (ESCA) (Gunther *et al.,* 2002; Hercules, 2004; Artyushkova, 2010; Hajati and Tougaard 2010).

3. Chemical imaging of ion mobility in tight formations

Combining microprobe techniques allows us to characterize the physical structure and chemical nature of a given heterogeneous porous medium, *e.g*. a tight clay formation. At the same time, chemical images documenting the evolution of reactive transport plumes spreading in the heterogeneous structure are obtained. Consequently, the relation between the heterogeneities observed and the expression of the reactive transport pattern can be established. In the present illustrative overview, the reactive transport of Cs in natural Opalinus Clay rock material will serve as an expounding scientific application. Opalinus Clay rock, which originated from marine Jurassic sediments, is a physically and chemically heterogeneous porous medium. Several European countries are currently evaluating similar tight argillaceous formations as potential host rocks and natural barrier systems in the context of nuclear-waste disposal (ANDRA, 2001; ONDRAF/NIRAS 2001; NAGRA, 2002).

To start, a first set of data will address the cases of one and two-dimensional microscopic images of reactive transport pattern. The data are related to a field-scale migration experiment conducted at the Mont Terri underground rock laboratory located in the northwestern part of Switzerland (http://www.mont-terri.ch/; Thury and Bossart, 1999; Bossart and Thury, 2007). A long-term diffusion experiment (DI-A) was performed at the underground site (Wersin *et al.,* 2004). Solutions containing multiple tracers were injected into a borehole. Tracers were allowed to migrate into the host rock for ~1 y. As a special feature compared to other field-scale tracer injection experiments, an over-core was excavated after completion of the injection part of the experiment. Several secondary (experimental) drill cores have been extracted from the over-core in a direction perpendicular to the injection borehole. This procedure provides direct access to multi-dimensional information from within the porous medium. Detailed information related to the migration experiment (and follow-up experiments) as well as the over-coring procedure can be found elsewhere (Wersin *et al.,* 2004, 2008; Gimmi *et al.,* 2014).

3.1. One-dimensional reactive transport pattern

A typical diamond wire-cut section of a secondary drill-core is depicted in Figure 1a. The interface between the quartz-filled injection borehole (left side) and the rock matrix is clearly visible. At first, synchrotron-based microscopic X-ray fluorescence (micro-XRF) and LA-ICP-MS were employed to record one-dimensional line scans. The Cs concentration profiles deduced from selected line scans along the direction of migration are depicted in Figure 1b in a semi-logarithmic representation. The plateau region (up to a migration distance of ~15 mm) adjacent to the injection borehole as well as the forefront of the diffusion front reaching into the pristine rock material is

readily apparent. Accordingly, Cs diffused ~20 mm into the rock material during the migration period of ~12 months. Both techniques, micro-XRF and LA-ICP-MS, yielded results which are in close agreement. The 'apparent' noise in the Cs diffusion profiles corresponds to reproducible variations in the local Cs concentrations arising from the chemical micro-heterogeneity of the Opalinus Clay rock. The deflections from the mean value of the diffusion profile are not single-point noise, but systematic drops and rises with typical widths of a few tens of micrometers (a detailed illustration was given by Wang *et al.,* 2011). The observed minor deviations between the two independent micro-analytical techniques are mainly due to a spatial offset of the two reported line scans by ~25 μm as well as by differences in the extension of the microscopic measurement voxels (micrometric differences in spot sizes and probing depths for LA-ICP-MS and synchrotron micro-XRF). Nevertheless, the close spatial correlation of the 'spike pattern' obtained using the two independent analytical techniques provided further evidence of the systematic (*i.e.* geochemically induced) nature of the Cs-concentration variations. The strong impact of the local geochemical characteristics of the porous medium on the reactive transport pattern is further substantiated by the concurrent concentration modulations observed for several major elements such as calcium (Ca), iron (Fe), or potassium (K) (Wang *et al.,* 2011, 2012; see also below).

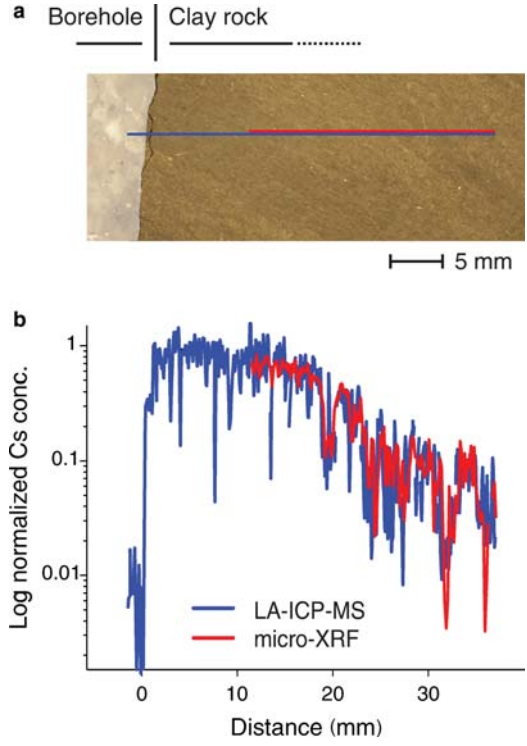

Figure 1. One-dimensional analysis of the reactive solute transport of Cs in Opalinus Clay rock: (a) Image of the borehole–clay rock interface section. The location of the one-dimensional line scans is indicated. (b) Cesium diffusion profile in semi-logarithmic representation as measured by micro-XRF and LA-ICP-MS.

3.2. Two-dimensional reactive transport pattern

A further improved understanding of the relationship between local geochemistry and reactive transport pattern can be gained by extending the analysis from one to two dimensions. Examples of two-dimensional chemical images are depicted in Figures 2b–f for selected elements including Cs. These extended maps were recorded at the

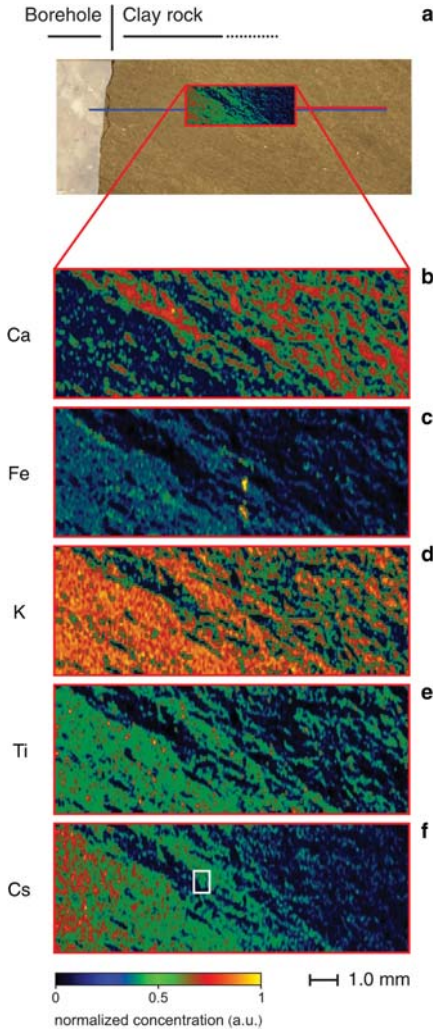

Figure 2. Two-dimensional reactive solute transport of Cs in Opalinus Clay rock: (a) Image of a section of the borehole–clay rock interface. The location of the two-dimensional chemical images is indicated. (b–f) Chemical images recorded at the forefront of the diffusion depicting semi-quantitatively the local concentration of Ca, Fe, K, Ti, and Cs, respectively; the images represent relative concentrations. The microscopic geochemical heterogeneity and pronounced elemental correlations are observed readily. The square in part f indicates the location of the high-resolution image shown in Figure 3.

front of the diffusion profile. The combined consideration of elemental distribution maps yields basic information about the composition and related structure of the tight clay formation. Distinct distribution patterns were established for all the elements investigated (Figure 2). Two major types of domains were observed. Calcium-rich patches were found within a material rich in Ti and K (but also Si and Al among others; data not shown). The domain features observed exhibited a characteristic length scale in the order of 100 μm. The different domains are separated by sharp boundaries. As can be seen from the high-resolution maps depicted in Figure 3, the different elemental concentrations are changing by about one order of magnitude within a few micrometers at the boundaries. Element concentrations within each distinct domain are rather homogeneous. The distribution pattern for Ti is slightly different. An elevated, but rather constant, Ti background concentration was detected and is studded with local maxima ('titanium hot spots') which are $<\sim 20$ μm across.

Elemental micro-analysis (micro-XRF) can be complemented by information about the presence and distribution of crystalline phases provided by spatially resolved micro X-ray diffraction (micro-XRD). Analysis of comparable Opalinus Clay rock samples by microscopic diffraction imaging with simultaneous micro-XRF microscopy revealed characteristic distributions of mineral phases congruent with the element pattern observed using micro-XRF: Ca-rich domains exhibited predominant calcium carbonate ($CaCO_3$, calcite form) while in the regions of enhanced Ti and K, clay minerals, especially illite, are localized. Relating the sampling voxel size (a few μm^3) to the number of XRD reflection spots observed, a broad size distribution of the calcite single crystals covering the range up to micrometer(s) can be established. The

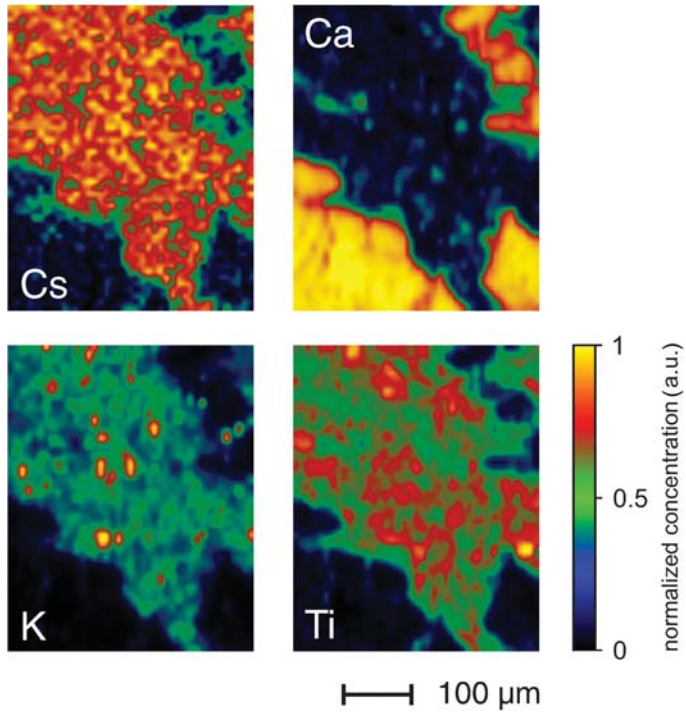

Figure 3. High-resolution image of part of Figure 2 detailing the geochemical heterogeneity expressed by micro-domains and sharp domain boundaries. Relative concentrations are shown.

individual calcite single crystallites are considerably smaller than the local dimension of the Ca-rich domain. In addition, the Fe-rich hot spots are identified as nano- and micro-crystalline pyrite conglomerates. Based on the characteristics of the elemental distributions maps in combination with the XRD-based phase identification, the host-rock materials are said to correspond to a complex mineral composite with an interlinked three-dimensional network structure. Calcite-dominated domains are embedded in a surrounding clay-rich matrix. Subsequent three-dimensional analysis by synchrotron-based micro-tomography confirmed experimentally the proposed three-dimensional network structure (see below).

In Figure 2f the diffusion front of Cs is clearly visible. The observed migration pattern is clearly controlled by the chemical heterogeneity of the rock material. Comparing the Cs pattern to the distribution of other elements reveals pronounced correlations and anti-correlations, respectively. Positive correlations between Cs and K as well as Cs and the diffuse Ti background can be established; Cs and Ca, on the other hand, are anti-correlated. Similarly, the pyrite phases, commonly among the most reactive phases in subsurface porous media, seem to play a negligible role in terms of the retention of Cs within the Opalinus Clay rock. Enhanced Cs levels cannot be established within, at the interface with, or close to the pyrite clusters.

The observation of distinguished correlations between the spatial distribution of Cs and the distribution pattern of major or trace constituent elements of the Opalinus Clay rock material yields important information regarding the identification of the reactive solid phase(s) controlling the retardation of Cs. Two types of domains, calcite- and pyrite-dominated, have the lowest local Cs concentrations and are, therefore, not involved in Cs retention processes (Figures 2, 3). This chemical passivity observed *in situ* within domains of the porous medium could be induced by different causes. First, the materials present within these domains can indeed be chemically inert, at least regarding geochemical reactions relevant to the chemistry of Cs. Note, however, the same materials can potentially exhibit a pronounced chemical reactivity in relation to other chemical species (*e.g.* the pyrite domains and redox-sensitive tracers). Second, reactions can be rather slow, and controlled kinetically, and yet not express a detectable build-up of reaction products despite the reaction time of >12 months. In general, reaction kinetics is a crucial factor in nearly all reactive-transport studies. The ability to record time series of undisturbed systems (see below) would be highly beneficial in tackling this important point. A third cause can be related to a constricted accessibility of the non-reactive domains. Domains can be excluded from the solute flow field, *e.g.* through the absence of porosity, surface passivation, or surface-coating phenomena. Microscopic chemical imaging can contribute to the resolution of the relevance of these potential causes. For the calcite domains, neither characteristic elemental patterns (by micro-XRF) nor crystalline phase distributions (by micro-XRD) are observed systematically at the domain boundaries. Consequently, surface passivation or coating phenomena can be ruled out. In the case of pyrite, however, combined micro-XRF and micro-XRD with high spatial resolution revealed the characteristic embedding of clusters of pyrite (micrometers long) within a cementing calcite matrix. This observation is consistent with results obtained by electron microscopy (Mäder and Mazurek, 1998; Fernández *et al.,* 1999; Pearson *et al.,* 2003; Lerouge *et al.,* 2011). The reactivity of pyrite may indeed be limited because of these coatings. The absence of, or extremely low, porosity can only be expected in the case of the domains being large single crystals. Chemical imaging by micro-XRD showed the mean single-crystal size distribution for the calcite to be significantly less than the typical extension of the non-reactive domains (compare the structural imaging results obtained by 'conventional' absorption contrast tomography, discussed below). In addition, for highly reactive, but non-porous grains, reactions should take place at least at the outer surface resulting in a characteristic shell-like chemical pattern. In the present system, however, the micro-XRF two-dimensional imaging has not revealed an elevated Cs concentration at the interfaces, or in the closer vicinity of the non-reactive domains. To obtain further evidence of the potential role of restricted accessibility of domains, the local effective diffusivity within and across the non-reactive (and the reactive) domains can be investigated itself by two approaches.

The first strategy corresponds to an indirect local measurement by analyzing physically the local porosity, *e.g.* by Focused Ion Beam (FIB) tomography or high-resolution X-ray-based tomography techniques (Keller *et al.,* 2011; Houben *et al.,* 2013; Noiriel, 2015). The second approach is again based on direct imaging of chemical

species. Corresponding opportunities include the spatially resolved analysis of inert tracers, or the direct analysis of the mobility of the pore water (*e.g.* by neutron techniques, see more below). All of the complementary information available in this case indicates that the calcite and the pyrite domains are part of the flow field but chemically inert with respect to Cs retention.

On the other hand, the Cs distribution pattern is almost identical to the distribution patterns of K or Ti. The local concentration measured within these domains is largely enhanced compared to values estimated based on the injected tracer concentration and typical porosities commonly measured for Opalinus Clay rock materials. Such a local enrichment can only be rationalized based on chemical reactivity in this domain. Based on the microscopic XRF and XRD results, one can speculate that either a K-rich clay mineral (*e.g.* illite, present at levels up to 30 wt.% in Opalinus Clay rock) or another (amorphous) phase associated with the clay material, *e.g.* an amorphous titanium oxide surface coating, is the most reactive phase with respect to Cs uptake. The association between Ti and clay minerals clearly results in a strong spatial correlation between Ti and indicator elements for clay minerals such as K. As the size of these reactivity domains (Johnston, 2010) is smaller than the probing X-ray beam (a few μm^2), final identification of the reactive phase cannot be obtained solely based on elemental correlations. Molecular-level information regarding the speciation of Cs retained in the Opalinus Clay rock is required.

Knowledge of the molecular environment around Cs, its coordination and bonding, can be extended by means of spectroscopic techniques. X-ray absorption spectroscopy (XAS) represents a prominent and powerful example of such a spectroscopic tool (for an introduction and further details see Teo, 1986; Koningsberger and Prins, 1988; Bunker, 2010; Henderson *et al.,* 2014; Newville, 2014). In the present system, X-ray absorption spectroscopy provided convincing evidence that intercalation ('trapping') of Cs into clay interlayer spaces was the dominant retention mechanism (Wang *et al.,* 2011). The spectroscopic signatures observed are inconsistent with outer-sphere sorption complexes and aqueous complexes, but at the same time, a direct covalent chemical bonding of Cs to a solid surface (*e.g.* clay, pyrite) can also be ruled out. Similarly, the possibility of incorporation of Cs in a secondary phase by precipitation can also be rejected based on the spectroscopic results. However, the observed characteristic distortion of the first coordination sphere around Cs, a splitting of the nearest coordination sphere into two distinct pairs of O–Cs bonding distances (Wang *et al.,* 2011), would be expected for Cs intercalation into clay interlayers as shown by experiments (Bostick *et al.,* 2002) and computational analysis (Smith, 1998; Sutton and Sposito, 2001, 2002; Nakano *et al.,* 2003).

Although not directly applicable in the present case of Cs retention in Opalinus Clay rock, note again the value of combining X-ray absorption spectroscopy and microscopic imaging (= spectromicroscopy) (Ade *et al.,* 1992; Sutton *et al.,* 1995; Grolimund *et al.,* 2004). The fine structure of an absorption edge reveals a variety of information about the molecular and electronic structure of the absorber atom. The differences in the spectroscopic signatures of different chemical species represent chemical contrast which can be used to record two- (maybe even three-) dimensional images depicting chemical

information such as oxidation states, mineral phases, or different molecular species (Pickering *et al.,* 2000; Rau *et al.,* 2003; Grolimund *et al.,* 2004; Kemner *et al.,* 2004; Mayhew *et al.,* 2011; Meirer *et al.,* 2011; Grafe *et al.,* 2014).

3.3. Three-dimensional reactive transport pattern

As documented above, the two-dimensional chemical imaging has clearly demonstrated its unique potential to elaborate heterogeneity-reactivity relationships. Two main limitations remain, however. First, the methodological concepts commonly involve sample sectioning, making the sample preparation step of the investigation destructive in terms of system integrity. Repeated *in situ* investigations of the very same system are, therefore, precluded. Second, two-dimensional analysis cannot provide information regarding the interconnection of heterogeneities (*e.g.* cracks, chemical domains, *etc*.). Considering reactive transport in three-dimensional systems, however, these interconnections are among the most critical factors determining transport patterns. Both limitations can be eliminated by non-destructive, full three-dimensional physical and chemical imaging. X-ray as well as neutron techniques can be considered as being non-destructive and non-invasive. Consequently, corresponding three-dimensional, tomographic methods have been developed and are 'routinely' available (Bleuet *et al.,* 2010). This is primarily true for physical analysis, methodological concepts delivering chemical information in three-dimensional space have only recently been emerging (Tsuchiyama *et al.,* 2005; Ludwig *et al.,* 2010; Sakdinawat and Attwood, 2010; King *et al.,* 2014).

Using this chemical tomographic approach, the three-dimensional distribution of a given element can be obtained by element-specific tomography, also referred to as absorption edge difference tomography (Tsuchiyama *et al.,* 2005; Gualda *et al.,* 2010). The underlying concept is illustrated in Figure 4. The energy tunability of the X-ray radiation delivered at synchrotron facilities allows the recording of tomograms at particular energies. Most interesting are couples of tomograms collected just below and above the specific absorption edge of an element of interest. In the example shown in Figure 4a, two types of Cs absorption edges, recorded with different spectral resolutions, are shown. Employing a double crystal spectrometer, in the present case equipped with Si(311) crystals, provides high spectral resolution (narrow bandpass), while a larger photon flux can be obtained using a multilayer monochromator, although at the penalty of a lower spectral resolution. As tomographic investigations are generally photon flux limited, a broad bandpass, high flux, but lower spectral resolution configuration is commonly preferred. Despite the reduced spectral resolution, the chemical contrast is not substantially affected as long as no other elemental edge falls within the energy difference window used. Across its absorption edge towards higher energies, the resonating element reveals an increase in the X-ray absorption coefficient, while all other elements exhibit a much smaller decrease in their cross sections over the energy interval probed. Consequently, the observation of voxels with elevated local absorption coefficients in the high-energy tomogram as compared to the low-energy tomogram points directly to the presence of element(s) exhibiting absorption resonances

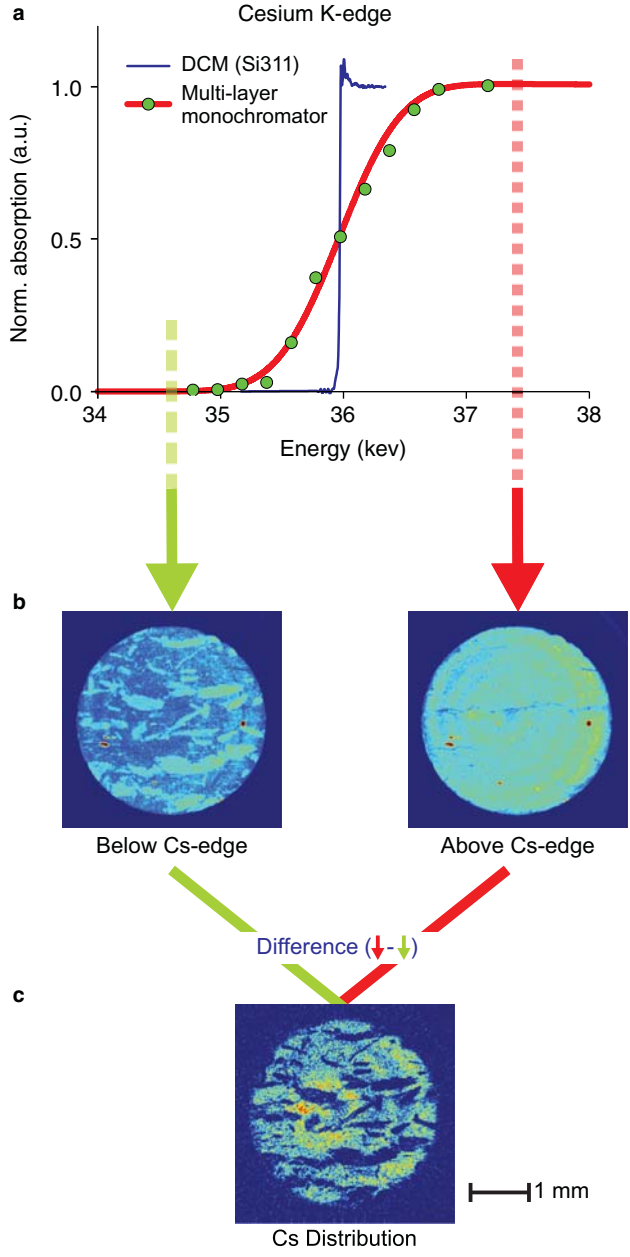

Figure 4. Absorption edge contrast tomography of an Opalinus Clay rock pillar after Cs in-diffusion: (a) Cs K-edge absorption spectrum recorded with a high flux, broad bandwidth multilayer monochromator compared to a spectrum collected using a double crystal monochromator equipped with Si(311) crystals providing high spectral resolution. (b) Two horizontal slices corresponding to identical volumes of the sample reconstructed from tomograms recorded above and below the Cs K-edge. (c) Semi-quantitative local Cs concentration.

in the energy interval probed. Even in the case of complex and heterogeneous structures, the local 'intensity' differences in such pairs of tomograms can, as a first approximation, be attributed solely to the local concentration of the absorbing element.

The absorption-edge difference tomography described was employed to investigate the *in situ* three-dimensional elemental distribution of Cs after in-diffusion into a confined cylindrical Opalinus Clay rock sample. The resulting effect in absorption contrast across the Cs K-edge is illustrated in Figure 4b depicting corresponding reconstructions of horizontal tomographic slices at identical height of the cylindrical sample. The left image corresponds to a slice collected using X-ray photons with an energy lower than the Cs K-edge, while the right image depicts the identical volume slice as 'seen' with X-rays of an energy just above the Cs absorption edge. The difference in the local absorption coefficients observed in these two reconstructions is shown in Figure 4c and is directly proportional to the local Cs concentration.

The spatial resolution of the tomographic data shown in Figure 4 is $\sim$3 μm (pixel resolution). This resolution is definitely not the best figure of merit of modern X-ray tomography instrumentation and methodologies (Kanitpanyacharoen *et al.,* 2013; Bonanno *et al.,* 2015), but corresponds to a compromise among spatial resolution, data-collection time, and obtainable field of view. The selected resolution is, however, just about sufficient to identify potential transport relevant, micro-scale features such as grain coatings or secondary precipitations.

The reconstructed three-dimensional results of the entire volume are shown in Figures 5 and 6. To enhance the visibility of the complex three-dimensional features, Figure 5 accentuates vertical slices along the direction of migration, while in Figure 6 the corresponding horizontal cuts are emphasized. From the 'below-the-edge' tomogram, the physical structure can be deduced (Figures 5a,b and 6a,b). Three main components are readily apparent through three dominant contrast levels. The investigated Opalinus Clay rock sample does indeed exhibit an interlinked three-dimensional network structure. This finding, based on physical imaging of structural features, is consistent with the conclusions drawn from the two-dimensional chemical imaging presented above. The individual domains can be separated by segmentation. The extension in space of the individual domains is illustrated in Figures 5c–e and 6c–e. The chemical 'identities' of these components can be assigned based on complementary chemical microprobe analysis (micro-XRF, micro-XRD). Such chemical imaging work can be conducted either destructively by analyzing extracted thin sections prepared following final sample disintegration or in a non-destructive manner by probing the outer surface of the rock object. Furthermore, complementary chemical tomography methods such as micro-XRF tomography and micro-XRD tomography (Baruchel *et al.,* 2008; Bleuet *et al.,* 2010; de Jonge and Vogt 2010; Alvarez-Murga *et al.,* 2012; King *et al.,* 2014) can be applied to gain insights into the internal chemical properties. Based on such complementary physical and chemical analysis, the full three-dimensional structure and interconnections of the heterogeneous porous medium – in the present case calcium carbonate domains embedded in a surrounding clay-rich matrix – can be mapped and reproduced.

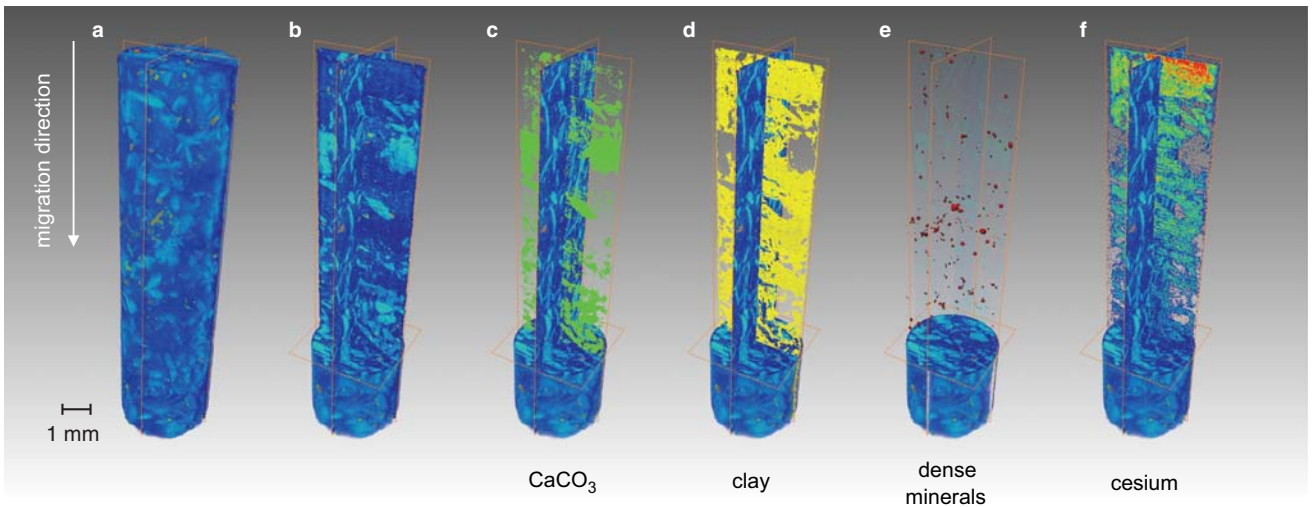

Figure 5. Three-dimensional visualization of undisturbed reactive solute transport pattern and geochemical heterogeneity in an Opalinus Clay rock sample. (a) Tomographic reconstruction based on absorption contrast. Three predominant constituents are observed. (b) Orthogonal vertical slices revealing the interior of the sample volume. (c–e) Representation of the individual components isolated by segmentation. The chemical nature of the components was assigned based on combined micro-XRF and micro-XRD results. (f) Three-dimensional visualization of the undisturbed reactive transport pattern of Cs developed after in-diffusion obtained by absorption-edge contrast tomography.

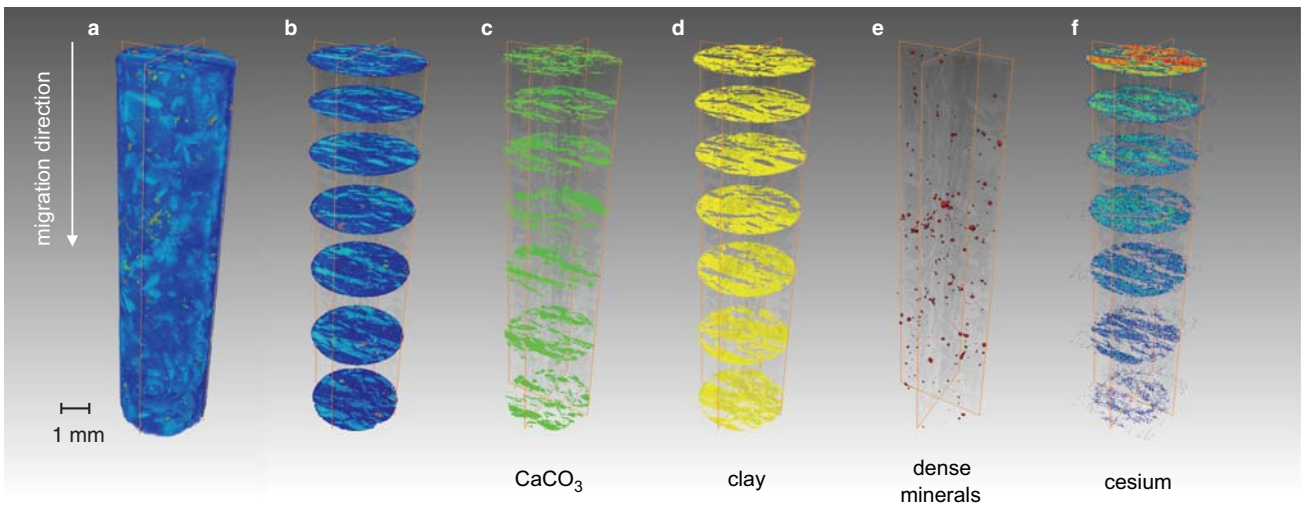

Figure 6. Three-dimensional visualization of undisturbed reactive solute transport pattern and geochemical heterogeneity in an Opalinus Clay rock sample. (a) Tomographic reconstruction based on absorption contrast. (b) Horizontal slices revealing the interior of the sample volume. (c–e) Representation of the individual components isolated by segmentation. (f) Three-dimensional visualization of the undisturbed reactive transport pattern of Cs developed after in-diffusion obtained by absorption-edge contrast tomography.

Most important, however, the absorption edge difference tomogram yields the corresponding full three-dimensional Cs diffusion plume developed in this complex, heterogeneous clay formation (Figures 5f and 6f). Considering first only a general view, the Cs distribution pattern shows a decreasing Cs concentration along the migration direction as one would expect for the case of in-diffusion (with constant Cs concentration at the boundary). However, analyzing the spatially resolved three-dimensional reactive transport pattern reveals several peculiarities. First, pronounced void volumes without detectable local Cs content are observed even close to the inlet boundary. Second, 'fingering' features are seen at the forefront of the diffusion front. Further, a close link between the geochemical heterogeneity (Figures 5c–e, 6c–e) and the reactive transport pattern (Figures 5f, 6f) can be recognized over the entire volume.

The data presented represent a rather unique insight into a reactive, undisturbed porous medium. This full three-dimensional, concurrent visualization of both a reactive solute transport pattern and the corresponding mineralogical micro-structures for the entire porous medium allows the user to relate local structural and chemical properties to the reactive transport pattern developed. Highly reactive components of the stationary phase can be identified and distinguished from inert materials. This represents a fundamental step toward clarification of the relevant chemical processes limiting the migration of hazardous substances.

The availability of such 'realistic' representations of the physical and chemical complexity allows the user to investigate the importance of (inevitable) simplifications and approximations implemented in reactive transport models. As an example, the relevance of artefacts introduced by applying a simple homogeneous and isotropic transport model to such a heterogeneous system can be analyzed by direct comparison to 'real-world observation.' The failure of homogeneous porous medium models to predict or simulate reactive transport experiments is addressed repeatedly in the literature (*e.g.* Van Loon and Jakob, 2005). The ability to represent the complexity of reactive transport systems with higher resolution and with additional dimensions opens up new opportunities to disentangle physical non-idealities such as variable local porosities and various chemical phenomena including reaction kinetics, sorption non-linearities, or competition effects.

4. Neutron imaging

Aside from the reactive stationary phase and the reactive solute, the mobile porewater is another key subject in terms of reactive (solute) transport. Clearly, the mobility of the porewater represents one of the most fundamental processes in the context of transport of chemicals in porous media. Motivated by its importance, a broad range of experimental approaches has been used to characterize the variability of local effective diffusivity (and connectivity) in heterogeneous materials. Approaches which are mostly indirect and based on pore-space analysis are considered, however (Keller *et al.,* 2011; Houben *et al.,* 2013).

The unique potential of neutron imaging (Anderson *et al.,* 2009) as a direct probe of solute mobility in a complex porous medium is shown by an investigation examining

the mobility of the mobile transport medium itself in a fully saturated tight formation. Based on its pronounced contrast toward hydrogen, neutron radiography can be used to visualize the diffusion of pore water even in saturated porous media. Diffusion properties of porewater within clay-rock material can be studied *in situ* by exchanging H_2O (light water) for its chemical analogue D_2O (heavy water). Hydrogen and deuterium have considerable differences in their neutron cross sections, providing a microscopic isotope contrast for imaging. Within a first series of experiments conducted at the cold neutron imaging beamline, ICON, at the Swiss spallation neutron source SINQ (Kaestner *et al.,* 2011), the focus was on the impact of the anisotropy of the porous medium. Clay rocks are anisotropic materials due to sedimentation and compaction processes. To emphasize the effects of anisotropy, geochemically rather uniform subsamples of the Opalinus Clay rock material with well-defined bedding plane structures were used. The geometry of these subsamples were chosen such that the different orientations of the bedding planes were parallel to, perpendicular to, and tilted with respect to the direction of migration. A representation of the sample system is provided in Figure 7a by a neutron radiography image. On top of the confined Opalinus Clay rock cylinder, a head reservoir initially filled with D_2O serves as a source for infiltration and replacement of the H_2O porewater initially present in the tight formation. To avoid evaporation during the experiment, the system has to be sealed.

The D_2O from the top reservoir diffuses into the porous medium replacing the H_2O-dominated pore water. The diffusion of D_2O into the clay stone sample can be followed directly by monitoring the local increase in neutron absorption in the rock material. At the same time, the reduction in the neutron contrast in the D_2O top reservoir observed

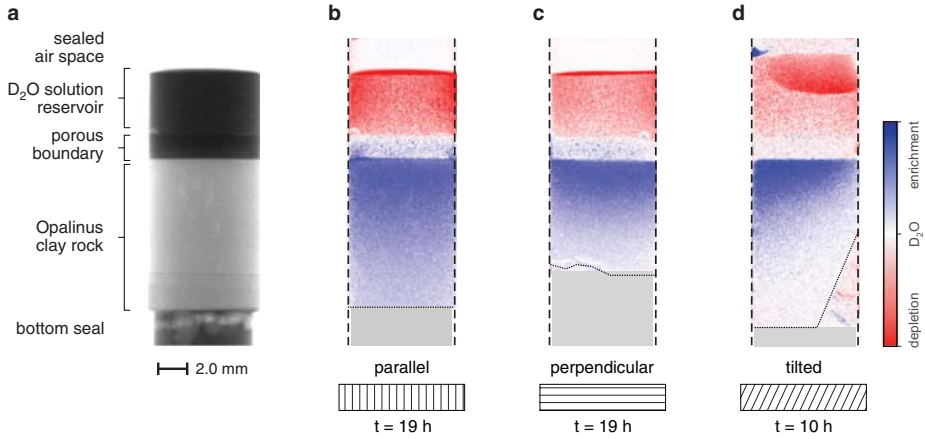

Figure 7. Isotopic imaging of the mobility of water in a saturated Opalinus Clay-rock sample by neutron radiography. (a) Neutron radiographic image depicting the sealed experimental sample system. (b–d) Isotopic contrast images after D_2O in-diffusion into three fully H_2O-saturated Opalinus Clay rock samples with bedding planes in different orientations. The effect of anisotropy is visible in the isotopic contrast images by the different shapes and position of the D_2O–H_2O exchange front (reflected by the positive isotope contrast given in blue). The geometrical orientation of the bedding planes is sketched at the base of each figure panel.

can be used to measure the total flux of H_2O porewater out of the porous medium. Note that due to complex multiple scattering phenomena, a full quantitative analysis of neutron imaging data presents a challenge (Hassanein *et al.,* 2005*,* 2006, 2008) and the data presented must be considered as semi-quantitative only.

Figures 7b–d show the differential neutron absorption for the three Opalinus Clay samples with the bedding planes oriented parallel to, perpendicular to, and tilted with respect to the direction of migration. An increase in neutron absorption compared to the initial situation at time zero is indicated by a blue contrast, while depletion is represented by a red color. For all three solid samples a clear negative difference is observed, reflecting the diffusion of D_2O into the rock samples. The corresponding out-diffusion of H_2O into the reservoir is manifested by a decreasing neutron absorption over time of the reservoir solution (red color). For all three samples a gradient from the reservoir boundary into the porous medium is established corresponding to the diffusion profile. Clear differences concerning the extension and shape of diffusion profiles are apparent for the different geometries. Note, though, that while the systems with perpendicular and parallel orientations were running for 19 h, the experimental time for the tilted system was limited to 10 h. The image of the tilted system was further complicated by the formation of a condensation droplet in the sealed headspace and movements of the meniscus at the solution reservoir–air interface resulted in a structured pattern of the reservoir. Nevertheless, the differences observed in diffusion velocities and profiles developed can be related directly to the anisotropic structural properties of the porous medium. The H_2O–D_2O exchange front advanced nearly twice as quickly for the case of diffusion along (parallel to) the bedding planes. The differences observed are in qualitative agreement with diffusion properties measured by through diffusion experiments (Van Loon *et al.,* 2004). The case of tilted bedding planes evolves according to the coupled diffusion vectors parallel and perpendicular to the bedding.

As demonstrated based on this fairly simple system, the methodology can be transferred easily to more complex systems, such as the study of effective local porosities in heterogeneous materials (*e.g.* the clay-calcite domain structures discussed previously), or the study of pore-clogging phenomena induced by secondary-phase formation occurring at reactive interfaces such as clay rock–cement boundaries (Dahn *et al.,* 2014; Jenni *et al.,* 2014; Chagneau *et al.,* 2015; Shafizadeh *et al.,* 2015). The data presented in Figures 7b–d correspond to snapshots at the end of the experiment. The non-destructive nature of the experimental approach, however, allows the user to monitor *in situ* the temporal evolution of the water-migration pattern in the saturated tight formation over the entire course of the diffusion experiment.

5. Conclusions and outlook

Recent progress and achievements in the field of two- and three-dimensional chemical imaging of reactive transport phenomena in natural and engineered tight clay formations using various neutron- and synchrotron-radiation-based microprobe

techniques as well as novel laboratory-based microprobe-analytical techniques have been demonstrated.

Tight clay formations exhibit pronounced heterogeneities at various length scales. Both classes of heterogeneities, physical and chemical, must be considered in order to advance understanding of fundamental reactive (solute) transport processes. The multi-dimensional multi-modal imaging conducted of the transport system shows clearly that these system heterogeneities are indeed transport relevant. Physical heterogeneities such as local density or porosity variations will primarily affect non-reactive tracers. In contrast, chemical heterogeneities including local chemical composition, reactive mineral-phase distribution, or redox domains will influence the local mobility of reactive tracers. Consequently, each individual tracer will be impacted by the system heterogeneities in its particular, individual manner.

The modern analytical techniques employed such as synchrotron-based micro-XRF, spectromicroscopy or micro-tomography, neutron imaging as well as laboratory-based microprobe techniques are capable of providing new insights into reactive diffusion processes occurring in multi-domain micro-structured porous media. Most importantly, these modern methods can yield 'inside' information on the heterogeneous distribution of chemical properties and their interconnection. Combined with the capability to image up to three-dimensional reactive transport patterns, heterogeneity-reactivity relationships can be derived.

Most relevant in terms of future prospects, the X-ray and neutron techniques can be considered as non-destructive and non-invasive techniques (at least in most cases). This important feature allows the recording of multiple, subsequent images of undisturbed profiles as a function of evolution, making up a 'reactive transport movie.' Such time-resolved, chemical imaging can potentially be used to conduct dynamic, *in situ* investigations elucidating the diffusion of water and inert tracers, as well as the mobility of reactive aqueous species. One could even envision non-destructive investigations which provide details of phenomena acting on longer timescales such as secondary-phase formation and pore clogging in a sequential, undisturbed manner.

Available time-resolved 3D chemical imaging and structure analysis offer opportunities for advanced 3D transport modeling taking into account the compositional heterogeneity of the samples at a (sub)-micrometer scale consistent with the experimental observations. The rapid development of analytical imaging techniques obviously has to go along with novel data analysis and modeling approaches. Through a model-based interpretation of 4D experimental results, one can expect new fundamental knowledge regarding relevant mechanisms of reactive (solute) transport phenomena and chemical interactions in reactive porous media such as tight clay formations.

Acknowledgments

Initial micro-XAS and XAS experiments were performed at the Pacific Northwest Consortium/X-ray Operations and Research (PNC/XOR) beamline at the Advanced Photon Source (APS). Special thanks are due to Steven Heald (PNC/XOR) for excellent local

support. Additional micro-XRF- and micro-XRD-based imaging data were collected at the microXAS beamline, while the tomographic data were produced at the TOMCAT beamline, both beamlines hosted by the Swiss Light Source (SLS) operated by the Paul Scherrer Institute (PSI), Switzerland. Neutron imaging was performed using the ICON beamline of the Swiss Spallation Neutron Source (SINQ) at PSI. The LA-ICP-MS data sets were recorded at the analytical laboratories of the Trace Element and Micro Analysis Group of the Swiss Federal Institute of Technology Zurich (ETHZ), Switzerland. All facilities are gratefully acknowledged for providing beam time and related support.

Opalinus Clay sample material was provided by the Mont Terri Underground Rock Laboratory. Related efforts by and scientific discussion with Paul Wersin and Olivier Leupin were much appreciated. Partial financial support by the Swiss National Foundation is acknowledged (Project 200021-119779).

Guest editor: Thorsten Schäfer

The authors and editors are grateful to anonymous reviewers who offered very helpful input and suggestions. A list of all reviewers is given at the end of the preface for this volume.

References

Ade, H., Zhang, X., Cameron, S., Costello, C., Kirz, J., and Williams, S. (1992) Chemical contrast in X-ray microscopy and spatially resolved XANES spectroscopy of organic specimens. *Science*, **258**, 972–975.

Alvarez-Murga, M., Bleuet, P., and Hodeau, J.L. (2012) Diffraction/scattering computed tomography for three-dimensional characterization of multi-phase crystalline and amorphous materials. *Journal of Applied Crystallography*, **45**, 1109–1124.

Anderson, I.S., McGreevy, R.L., and Bilheux, H.Z. (2009) *Neutron Imaging and Applications*. Springer, New York.

ANDRA (2001) Dossier 2001 Argile. Progress report on feasibility studies & research into deep geological disposal of high-level, long-lived waste. Synthesis report. Paris, France.

Appelo, C.A.J., Van Loon, L.R., and Wersin, P. (2010) Multicomponent diffusion of a suite of tracers (HTO, Cl, Br, I, Na, Sr, Cs) in a single sample of Opalinus Clay. *Geochimica et Cosmochimica Acta,* **74**, 1201–1219.

Artyushkova, K. (2010) Structure determination of nanocomposites through 3D imaging using laboratory XPS and multivariate analysis. *Journal of Electron Spectroscopy and Related Phenomena*, **178**, 292–302.

Banhart, J., Borbely, A., Dzieciol, K., Garcia-Moreno, F., Manke, I., Kardjilov, N., Kaysser-Pyzalla, A.R., Strobl, M., and Treimer, W. (2010) X-ray and neutron imaging – Complementary techniques for materials science and engineering. *International Journal of Materials Research,* **101**, 1069–1079.

Baruchel, J., Bleuet, P. Bravin, A., Coan, P., Lima, E., Madsen, A., Ludwig, W., Pernot, P., and Susini, J. (2008) Advances in synchrotron hard X-ray based imaging. *Comptes Rendus Physique,* **9**, 624–641.

Bertsch, P.M. and Hunter, D.B. (2001) Applications of synchrotron-based X-ray microprobes. *Chemical Reviews*, **101**, 1809–1842.

Bleuet, P., Lemelle, L., Tucoulou, R., Gergaud, P., Delette, G., Cloetens, P., Susini, J., and Simionovici, A. (2010) 3D chemical imaging based on a third-generation synchrotron source. *Trac-Trends in Analytical Chemistry*, **29**, 518–527.

Bonanno, G., Coppo, S., Modregger, P., Pellegrin, M., Stuber, A., Stampanoni, M., Mazzolai, L., Stuber, M., and van Heeswijk, R.B. (2015) Ultra-high-resolution 3D imaging of atherosclerosis in mice with synchrotron differential phase contrast: a proof of concept study. *Scientific Reports*, **5**, 11980.

Bossart, P. and Thury, M. (2007) Research in the Mont Terri Rock laboratory: Quo vadis? *Physics and Chemistry of the Earth, Parts A/B/C* **32**(1–7), 19–31.

Bostick, B.C., Vairavamurthy, M.A., Karthikeyan, K.G., and Chorover, J. (2002) Cesium adsorption on clay minerals: An EXAFS spectroscopic investigation. *Environmental Science & Technology*, **36**, 2670–2676.

Bunker, G. (2010) *Introduction to XAFS. A Practical Guide to X-ray Absorption Fine Structure Spectroscopy*. Cambridge University Press, Cambridge, UK.

Cernik, M., Barmettler, K., Grolimund, D., Rohr, W., Borkovec, M., and Sticher, H. (1994) Cation-transport in natural porous-media on laboratory-scale – multicomponent effects. *Journal of Contaminant Hydrology*, **16**(4), 319–337.

Chagneau, A., Claret, F., Enzmann, F., Kersten, M., Heck, S., Made, B., and Schafer, T. (2015) Mineral precipitation-induced porosity reduction and its effect on transport parameters in diffusion-controlled porous media. *Geochemical Transactions,* **16**, 13, doi: 10.1186/s12932-015-0027-z

Cvetkovic, V., Cheng, H., Byegard, J., Winberg, A., Tullborg, E.L., and Widestrand, H. (2010) Transport and retention from single to multiple fractures in crystalline rock at Aspo (Sweden): 1. Evaluation of tracer test results and sensitivity analysis. *Water Resources Research*, **46**, W05505, doi: 10.1029/2009WR008013.

Dahn, R., Popov, D., Schaub, P., Pattison, P., Grolimund, D., Mader, U., Jenni, A., and Wieland, E. (2014) X-ray micro-diffraction studies of heterogeneous interfaces between cementitious materials and geological formations. *Physics and Chemistry of the Earth*, **70–71**, 96–103.

Dai, Z., Wolfsberg, A., Reimus, P., Deng, H., Kwicklis, E., Ding, M., Ware, D., and Ye, M. (2012) Identification of sorption processes and parameters for radionuclide transport in fractured rock. *Journal of Hydrology*, **414–415**, 220–230.

de Jonge, M.D. and Vogt, S. (2010) Hard X-ray fluorescence tomography — an emerging tool for structural visualization. *Current Opinion in Structural Biology*, **20**, 606–614.

Dieing, T., Hollricher, O., and Toporski, J. (2011) *Confocal Raman Microscopy*. Springer, Berlin.

Fernández, A.M., Turrero, M.J., Cózar, J., and Rivas, P. (1999) Analysis of the solid material and chemical characterisation of trace elements in squeezed porewaters from BWS-A4 and BWS-A5 Opalinus clay core material from the Mt. Terri Tunnel, Switzerland. (WS-C experiment), Mont Terri Project.

Geckeis, H., Schäfer, T., Hauser, W., Rabung, T., Missana, T., Degueldre, C., Mori, A., Eikenberg, J., Fierz, T., and Alexander, W.R. (2004) Results of the colloid and radionuclide retention experiment (CRR) at the Grimsel Test Site (GTS), Switzerland – impact of reaction kinetics and speciation on radionuclide migration. *Radiochimica Acta,* **92**, 765–774.

Giesen, C., Wang, H.A.O., Schapiro, D., Zivanovic, N., Jacobs, A., Hattendorf, B., Schuffler, P.J., Grolimund, D., Buhmann, J.M., Brandt, S., Varga, Z., Wild, P.J., Gunther, D., and Bodenmillerthat, B. (2014) Highly multiplexed imaging of tumor tissues with subcellular resolution by mass cytometry. *Nature Methods,* **11**, 417–422.

Gimmi, T., Leupin, O.X., Eikenberg, J., Glaus, M.A., Van Loon, L.R., Waber, H.N., Wersin, P., Wang, H.A.O., Grolimund, D., Borca, C.N., Dewonck, S., and Wittebroodt, C. (2014) Anisotropic diffusion at the field scale in a 4-year multi-tracer diffusion and retention experiment – I: Insights from the experimental data. *Geochimica et Cosmochimica Acta*, **125**, 373–393.

Goldstein, J., Newbury, D.E., Joy, D.C., Lyman, C.E., Echlin, P., Lifshin, E., Sawyer, L., and Michael, J.R. (2003) *Scanning Electron Microscopy and X-ray Microanalysis*. Springer, Berlin.

Grafe, M., Donner, E., Collins, R.N., and Lombi, E. (2014) Speciation of metal(loid)s in environmental samples by X-ray absorption spectroscopy: A critical review. *Analytica Chimica Acta*, **822**, 1–22.

Grolimund, D. and Borkovec, M. (2005) Colloid-facilitated transport of strongly sorbing contaminants in natural porous media: Mathematical modeling and laboratory column experiments. *Environmental Science & Technology* **39**, 6378–6386.

Grolimund, D., Senn, M., Trottmann, M., Janousch, M., Bonhoure, I., Scheidegger, A.M., and Marcus, M. (2004) Shedding new light on historical metal samples using micro-focused synchrotron X-ray fluorescence and spectroscopy. *Spectrochimica Acta Part B – Atomic Spectroscopy*, **59**, 1627–1635.

Gualda, G.A.R., Pamukcu, A.S., Claiborne, L.L., and Rivers, M.L. (2010) Quantitative 3D petrography using X-ray tomography 3: Documenting accessory phases with differential absorption tomography. *Geosphere*, **6**, 782–792.

Gunther, S., Kaulich, B., Gregoratti, L., and Kiskinova, M. (2002) Photoelectron microscopy and applications in surface and materials science. *Progress in Surface Science*, **70**, 187–260.

Hajati, S. and Tougaard, S. (2010) XPS for non-destructive depth profiling and 3D imaging of surface nanostructures. *Analytical and Bioanalytical Chemistry*, **396**, 2741–2755.

Hassanein, R., Lehmann, E., and Vontobel, P. (2005) Methods of scattering corrections for quantitative neutron radiography. *Nuclear Instruments & Methods in Physics Research Section a-Accelerators Spectrometers Detectors and Associated Equipment*, **542**, 353–360.

Hassanein, R., Meyer, H.O., Carminati, A., Estermann, M., Lehmann, E., and Vontobel, P. (2006) Investigation of water imbibition in porous stone by thermal neutron radiography. *Journal of Physics D – Applied Physics*, **39**, 4284–4291.

Hassanein, R., Vontobel, P., and Lehmann, E. (2008) *Correction Software Tool for Neutron Tomography*. Destech Publications, Inc., Lancaster, Pennsylvania, USA.

Henderson, G.S., de Groot, F.M.F., and Moulton, B.J.A. (2014) X-ray absorption near-edge structure (XANES) spectroscopy. Pp. 75–138 in: *Spectroscopic Methods in Mineralology and Materials Sciences* (G.S. Henderson, D.R. Neuville, and Downs, R.T., editors). Reviews in Mineralogy and Geochemistry, **78**, Mineralogical Society of America, Chantilly, Virginia, USA.

Hercules, D.M. (2004) Electron spectroscopy: Applications for chemical analysis. *Journal of Chemical Education*, **81**, 1751–1766.

Herrmann, A.M., Ritz, K., Nunan, N., Clode, P.L., Pett-Ridge, J., Kilburn, M.R., Murphy, D.V., O'Donnell, A.G., and Stockdale, E.A. (2007) Nano-scale secondary ion mass spectrometry – A new analytical tool in biogeochemistry and soil ecology: A review article. *Soil Biology & Biochemistry*, **39**, 1835–1850.

Hirschmugl, C.J. and Gough, K.M. (2012) Fourier transform infrared spectrochemical imaging: Review of design and applications with a focal plane array and multiple beam synchrotron radiation source. *Applied Spectroscopy*, **66**, 475–491.

Houben, M.E., Desbois, G., and Urai, J.L. (2013) Pore morphology and distribution in the shaly facies of Opalinus Clay (Mont Terri, Switzerland): Insights from representative 2D BIB–SEM investigations on mm to nm scale. *Applied Clay Science*, **71**, 82–97.

Jenni, A., Mader, U., Lerouge, C., Gaboreau, S., and Schwyn, B. (2014) In situ interaction between different concretes and Opalinus Clay. *Physics and Chemistry of the Earth*, **70–71**, 71–83.

Johansson, S.A.E., Campbell, J.L., and Malmqvist, K.G. (1995) *Particle Induced X-ray Emission spectrometry (PIXE)*, Wiley, New York.

Johnston, C.T. (2010) Probing the nanoscale architecture of clay minerals. *Clay Minerals*, **45**, 245–279.

Kaestner, A.P., Hartmann, S., Kühne, G., Frei, G., Grünzweig, C., Josic, L., Schmid, F., and Lehmann, E.H. (2011) The ICON beamline – A facility for cold neutron imaging at SINQ. *Nuclear Instruments and Methods in Physics Research Section A: Accelerators, Spectrometers, Detectors and Associated Equipment*, **659**, 387–393.

Kaestner, A.P., Trtik. P., Zarebandkouki, M., Kazantsev, D., Snehota, M., Dobson, K.J., and Lehmann, E.H. (2015) Recent developments in neutron imaging with applications for porous media research. *Solid Earth, Discussion papers*, **7**, 3481–3510.

Kanitpanyacharoen, W., Parkinson, D.Y., De Carlo, F., Marone, F., Stampanoni, M., Mokso, R., MacDowell, A., and Wenk, H.R. (2013) A comparative study of X-ray tomographic microscopy on shales at different synchrotron facilities, ALS, APS and SLS. *Journal of Synchrotron Radiation*, **20**, 172–180.

Katon, J.E. (1996) Infrared microspectroscopy. A review of fundamentals and applications. *Micron*, **27**, 303–314.

Keller, L.M., Holzer, L., Wepf, R., and Gasser, P. (2011) 3D geometry and topology of pore pathways in Opalinus clay: Implications for mass transport. *Applied Clay Science*, **52**, 85–95.

Kemner, K.M., Kelly, S.D., Lai, B., Maser, J., O'Loughlin, E.J., Sholto-Douglas, D., Cai, Z.H., Schneegurt, M.A., Kulpa, C.F., and Nealson, K.H. (2004) Elemental and redox analysis of single bacterial cells by X-ray microbeam analysis. *Science*, **306**, 686–687.

Kindness, A., Sekaran, C.N., and Feldmann, J. (2003) Two-dimensional mapping of copper and zinc in liver sections by laser ablation-inductively coupled plasma mass spectrometry. *Clinical Chemistry*, **49**, 1916–1923.

King, A., Reischig, P., Adrien, J., Peetermans, S., and Ludwig, W. (2014) Polychromatic diffraction contrast tomography. *Materials Characterization*, **97**, 1–10.

Kohler, M., Curtis, G.P., Kent, D.B., and Davis, J.A. (1996) Experimental investigation and modeling of uranium(VI) transport under variable chemical conditions. *Water Resources Research*, **32**, 3539–3551.

Koningsberger, D.C. and Prins, R. (1988) *X-ray Absorption, Principles, Applications, Techniques of EXAFS, SEXAFS and XANES*. John Wiley & Sons, New York.

Lehmann, E.H., Kaestner, A., Grunzweig, C., Mannes, D., Vontobel, P., and Peetermans, S. (2014) Materials research and non-destructive testing using neutron tomography methods. *International Journal of Materials Research*, **105**, 664–670.

Lehmann, P., Wyss, P., Flisch, A., Lehmann, E., Vontobel, P., Krafczyk, M., Kaestner, A., Beckmann, F., Gygi, A., and Fluhler, H. (2006) Tomographical imaging and mathematical description of porous media used for the prediction of fluid distribution. *Vadose Zone Journal* **5**, 80–97.

Lerouge, C., Grangeon, S., Gaucher, E.C., Tournassat, C., Agrinier, P., Guerrot, C., Widory, D., Fléhoc, C., Wille, G., Ramboz, C., Vinsot, A., and Buschaert, S. (2011) Mineralogical and isotopic record of biotic and abiotic diagenesis of the Callovian–Oxfordian clayey formation of Bure (France). *Geochimica et Cosmochimica Acta*, **75**, 2633–2663.

Liang, L., Rinaldi, R., and Schober, H. (2009) *Neutron Applications in Earth, Energy and Environmental Sciences*. Springer, Berlin.

Ludwig, W., King, A., Herbig, M., Reischig, P., Marrow, J., Babout, L., Lauridsen, E.M., Proudhon, H., and Buffiere, J.Y. (2010) Characterization of polycrystalline materials using synchrotron X-ray imaging and diffraction techniques. *JOM,* **62**, 22–28.

Mäder, U.K. and Mazurek, M. (1998) Oxidation phenomena and processes in Opalinus clay: Evidence from the excavation-disturbed zones in Hauenstein and Mt Terri tunnels, and Siblingen open clay pit. *Scientific Basis for Nuclear Waste Management XXI* (I.G. McKinley and C. McCombie, editors). Materials Research Society, **506**, pp. 731–739, Warrendale, USA.

Marcus, M.A. (2010) X-ray photon-in/photon-out methods for chemical imaging. *Trac-Trends in Analytical Chemistry*, **29**, 508–517.

Margaritondo, G., Hwu, Y.K., and Je, J.H. (2008) Nondestructive characterization by advanced synchrotron light techniques: Spectromicroscopy and coherent radiology. *Sensors*, **8**, 8378–8400.

Mayhew, L.E., Webb, S.M., and Templeton, A.S. (2011) Microscale imaging and identification of Fe speciation and distribution during fluid-mineral reactions under highly reducing conditions. *Environmental Science & Technology*, **45**, 4468–4474.

Meeussen, J.C.L., Kleikemper, J., Scheidegger, A.M., Borkovec, M., Paterson, E., Van Riemsdijk, W.H., and Sparks, D.L. (1999) Multicomponent transport of sulfate in a goethite-silica sand system at variable pH and ionic strength. *Environmental Science & Technology*, **33**, 3443–3450.

Meirer, F., Cabana, J., Liu, Y., Mehta, A., Andrews, J.C., and Pianetta, P. (2011) Three-dimensional imaging of chemical phase transformations at the nanoscale with full-field transmission X-ray microscopy. *Journal of Synchrotron Radiation*, **18**, 773–781.

NAGRA (2002) Project Opalinus Clay: Safety Report – Demonstration of disposal feasibility for spent fuel, vitrified high-level waste and long-lived intermediate-level waste (Entsorgungsnachweis) Wettingen, Switzerland, NAGRA. Nagra Technical Report NTB-02-05.

Nakano, M., Kawamura, K., and Ichikawa, Y. (2003) Local structural information of Cs in smectite hydrates by means of an EXAFS study and molecular dynamics simulations. *Applied Clay Science*, **23**, 15–23.

Newville, M. (2014) Fundamentals of XAFS. Pp. 33–74 in: *Spectroscopic Methods in Mineralology and Materials Sciences* (G.S. Henderson, D.R. Neuville, and R.T. Downs, editors). Reviews in Mineralogy and Geochemistry, **78**, Mineralogical Society of America, Chantilly, Virginia, USA.

Noiriel, C. (2015) Resolving time-dependent evolution of pore-scale structure, permeability and reactivity using X-ray microtomography. Pp. 247–285 in: *Pore-Scale Geochemical Processes* (C.I. Steefel,

S. Emmanuel, and L.M. Anovitz, editors). Reviews in Mineralogy, **80**, Mineralogical Society of America, Chantilly, Virginia, USA.

ONDRAF/NIRAS (2001) Technical overview of the SAFIR 2 report, Technical Report NIROND 2001. ONDRAF, Brussels, Belgium.

Pearson, F.J., Arcos, D., Bath, A., Boisson, J.-Y., Fernández, A.M., Gäbler, H.-E., Gaucher, E., Gautschi, A., Griffault, L., Hernán, P., and Waber, H.N. (2003) Mont Terri Project – Geochemistry of water in the Opalinus clay formation at the Mont Terri rock laboratory. Reports of the FOWG. Geology series.

Pickering, I.J., Prince, R.C., Salt, D.E., and George, G.N. (2000) Quantitative, chemically specific imaging of selenium transformation in plants. *Proceedings of the National Academy of Sciences of the United States of America*, **97**, 10717–10722.

Pinon, V., Mateo, M.P., and Nicolas, G. (2013) Laser-induced breakdown spectroscopy for chemical mapping of materials. *Applied Spectroscopy Reviews*, **48**, 357–383.

Prigiobbe, V. and Bryant, S.L. (2014) pH-dependent transport of metal cations in porous media. *Environmental Science & Technology*, **48**, 3752–3759.

Rau, C., Somogyi, A., and Simionovici, A. (2003) Microimaging and tomography with chemical speciation. *Nuclear Instruments & Methods in Physics Research Section B – Beam Interactions with Materials and Atoms*, **200**, 444–450.

Reed, S.J.B. (2010) *Electron Microprobe Analysis and Scanning Electron Microscopy in Geology*. Cambridge University Press, Cambridge, UK.

Sakdinawat, A. and Attwood, D. (2010) Nanoscale X-ray imaging. *Nature Photonics*, **4**, 840–848.

Sancey, L., Motto-Ros, V., Busser, B., Kotb, S., Benoit, J.M., Piednoir, A., Lux, F., Tillement, O., Panczer, G., and Yu, J. (2014) Laser spectrometry for multi-elemental imaging of biological tissues. *Scientific Reports* **4**, 7.

Schrofl, C., Mechtcherine, V., Kaestner, A., Vontobel, P., Hovind, J., and Lehmann, E. (2015) Transport of water through strain-hardening cement-based composite (SHCC) applied on top of cracked reinforced concrete slabs with and without hydrophobization of cracks – Investigation by neutron radiography. *Construction and Building Materials*, **76**, 70–86.

Shafizadeh, A., Gimmi, T., Van Loon, L., Kaestner, A., Lehmann, E., Maeder, U.K., and Churakov, S.V. (2015) Quantification of water content across a cement–clay interface using high resolution neutron radiography. *Physics Procedia*, **69**, 516–523.

Smith, D.E. (1998) Molecular computer simulations of the swelling properties and interlayer structure of cesium montmorillonite. *Langmuir*, **14**, 5959–5967.

Sutton, R. and Sposito, G. (2001) Molecular simulation of interlayer structure and dynamics in 12.4 angstrom Cs-smectite hydrates. *Journal of Colloid and Interface Science*, **237**, 174–184.

Sutton, R. and Sposito, G. (2002) Animated molecular dynamics simulations of hydrated caesium-smectite interlayers. *Geochemical Transactions*, **3**, 73–80.

Sutton, S.R., Bajt, S., Delaney, J., Schulze, D., and Tokunaga, T. (1995) Synchrotron X-ray-fluorescence microprobe – Quantification and mapping of mixed-valence state samples using micro-XANES. *Review of Scientific Instruments*, **66**, 1464–1467.

Teo, B.K. (1986) *EXAFS: Basic Principles and Data Analysis*. Springer, Berlin.

Thury, M. and Bossart, P. (1999) The Mont Terri rock laboratory, a new international research project in a Mesozoic shale formation, in Switzerland. *Engineering Geology*, **52**, 347–359.

Trainor, T.P., Templeton, A.S., and Eng, P.J. (2006) Structure and reactivity of environmental interfaces: Application of grazing angle X-ray spectroscopy and long-period X-ray standing waves. *Journal of Electron Spectroscopy and Related Phenomena*, **150**, 66–85.

Truchet, M., Merlin, J.-C., and Turrell, G. (1996) Raman microscopy and other local analysis techniques. Pp. 201–242 in: *Raman Microscopy* (G.T. Corset, editor). Academic Press, London.

Tsuchiyama, A., Uesugi, K., Nakano, T., and Ikeda, S. (2005) Quantitative evaluation of attenuation contrast of X-ray computed tomography images using monochromatized beams. *American Mineralogist*, **90**, 132–142.

Van Loon, L.R., Glaus, M.A., and Muller, W. (2007) Anion exclusion effects in compacted bentonites: Towards a better understanding of anion diffusion. *Applied Geochemistry*, **22**, 2536–2552.

Van Loon, L.R. and Jakob, A. (2005) Evidence for a second transport porosity for the diffusion of tritiated water (HTO) in a sedimentary rock (Opalinus clay-OPA): Application of through- and out-diffusion techniques. *Transport in Porous Media*, **61**, 193–214.

Van Loon, L.R. and Mibus, J. (2015) A modified version of Archie's law to estimate effective diffusion coefficients of radionuclides in argillaceous rocks and its application in safety analysis studies. *Applied Geochemistry*, **59**, 85–94.

Van Loon, L.R., Soler, J.M., Muller, W., and Bradbury, M.H. (2004) Anisotropic diffusion in layered argillaceous rocks: A case study with Opalinus clay. *Environmental Science & Technology,* **38**, 5721–5728.

Wang, H.A.O., Grolimund, D., Van Loon, L. R., Barmettler, K., Borca, C.N., Aeschimann, B., and Gunther, D. (2011) Quantitative chemical imaging of element diffusion into heterogeneous media using laser ablation inductively coupled plasma mass spectrometry, synchrotron micro-X-ray fluorescence, and extended X-ray absorption fine structure spectroscopy. *Analytical Chemistry*, **83**, 6259–6266.

Wang, H.A.O., Grolimund, D., Giesen, C., Borca, C.N., Shaw-Stewart, J.R.H., Bodenmiller, B., and Gunther, D. (2013) Fast chemical imaging at high spatial resolution by laser ablation inductively coupled plasma mass spectrometry. *Analytical Chemistry*, **85**, 10107–10116.

Wersin, P., Van Loon, L.R., Soler, J.M., Yllera, A., Eikenberg, J., Gimmi, T., Hernan, P., and Boisson, J.Y. (2004) Long-term diffusion experiment at Mont Terri: first results from field and laboratory data. *Applied Clay Science*, **26**, 123–135.

Wersin, P., Soler, J.M., Van Loon, L., Eikenberg, J., Baeyens, B., Grolimund, D., Gimmi, T., and Dewonck, S. (2008) Diffusion of HTO, Br^-, I^-, Cs^+, $^{85}Sr^{2+}$, and $^{60}Co^{2+}$ in a clay formation: Results and modelling from an in situ experiment in Opalinus Clay. *Applied Geochemistry*, **23**, 678–691.